Supplement of Atmos. Chem. Phys., 20, 12741–12759, 2020
https://doi.org/10.5194/acp-20-12741-2020-supplement

Supplement of

Emission of biogenic volatile organic compounds from warm and oligotrophic seawater in the Eastern Mediterranean

Chen Dayan et al.

Correspondence to: Eran Tas (eran.tas@mail.huji.ac.il) and Erick Fredj (erick.fredj@gmail.com)

S1. Availability of measured data and calibration

Measured data that did not pass the quality control were discarded, and only days with complete measured data were used for the analysis, resulting in 20 days of high-quality data.

Table S1*. Excluded measured data. Presented are data availability for the analysis and the reason for and percentage of excluded data.**

Reason	Percentage
Analyzed data (good data)	21%
Partial measurement days	5%
Poor quality	11%
File writing error	14%
Calibration error	8%
Measurement failure	11%
Blocked tube	28%
Electricity failure	2%

**Note that we also excluded measurements for DOY 257-260 from our analyses due to irregular meteorological conditions during this period, which resulted in an atypical diurnal profile shape, with no correlation between daytime temperature and biogenic volatile organic compound (BVOC) mixing ratios (see Sect. S4). "Failed calibration" refers to data which could not be properly calibrated due to failed calibration. In most cases failed calibration occurred due to dilution of the calibrated mixture with ambient air. "Poor quality" refers to data that corresponded with* *unrealistic mixing ratios or erroneous recording, such as the same value recorded repeatedly.*

According to the proton transfer reaction between the H_3O^+ reagent ions and a VOC producing protonated molecule RH^+, the signals of RH^+ ions $[RH^+]$ at the end of the drift tube can be described as follows

$$H_3O^+ + R \rightarrow RH^+ + H_2O \qquad \text{(Eq.1)}$$

$$[RH^+] = [H_3O^+]_0\left(1 - e^{-k[R]\Delta t}\right), \qquad \text{(Eq. 2)}$$

where k is the reaction rate constant, $[H_3O^+]_0$ is the signal of H_3O^+ ions before the reaction, $[R]$ is the number concentration of the VOC in the drift tube, and Δt is the reaction time for H_3O^+ traversing the drift tube. If the proton-transfer reactions only convert a small fraction of H_3O^+ into protonated molecule RH^+, $[RH^+]$ can be approximately expressed as (de Gouw et al., 2003; de Gouw and Warneke, 2007; Lindinger et al., 1998):

$$[RH^+] \approx [H_3O^+]k[R]\Delta t\ , \qquad \text{(Eq. 3)}$$

where $[H_3O^+]$ is the signal of the $[H_3O^+]$ ions after their exit from the drift tube.

Under a small H_3O^+ converted fraction, Eq. (3) can be used (De Gouw et.al. 2003) to estimate the compound $[R]$ concentration from the observed ion count rates, $I(RH^+)$ for RH^+ ions and $I(H_3O^+)$ for H_3O^+ ions and the reaction rate constant k as

$$[R] = \frac{1}{k\Delta t}\frac{I(RH^+)}{T(RH^+)}\left(\frac{I(H_3O^+)}{T(H_3O^+)}\right)^{-1} \qquad \text{(Eq. 4)}$$

The coefficients $T(RH^+)$ and $T(H_3O^+)$ are the transmission efficiencies for RH^+ and H_3O^+, respectively, and their values range between zero and one.

Table S2. *Compositions of the calibration gas standards. The standard was used in the calibrations. S norm indicates the normalized sensitivity, k_{theo} indicates the proton transfer reaction rate coefficients k reported by (Cappellin et al., 2012), while kobs indicates the effective proton transfer reaction rate coefficient observed during the field campaign. See also Fig. S1 for k_{theo}- k_{obs} regression.*

Compound	**S norm**	**m/z**	**k_{theo}** [10^{-9} cm^3 s^{-1}]	**k_{obs}** [10^{-9} cm^3 s^{-1}]
Acetaldehyde	**18.5**	45	3.17	3.16
Acetone	**22.8**	59	3.32	3.28
MVK+MACR	**21.6**	71	3.30	2.77
MEK	**25.9**	73	3.28	3.27
Benzene	**16.5**	79	1.93	1.99
Toluene	**19.8**	93	2.08	2.16
Xylene	**22.7**	107	2.26	2.28
TMB	**22.4**	121	2.40	2.10
D5	**40.5**	371	2.00	2.03

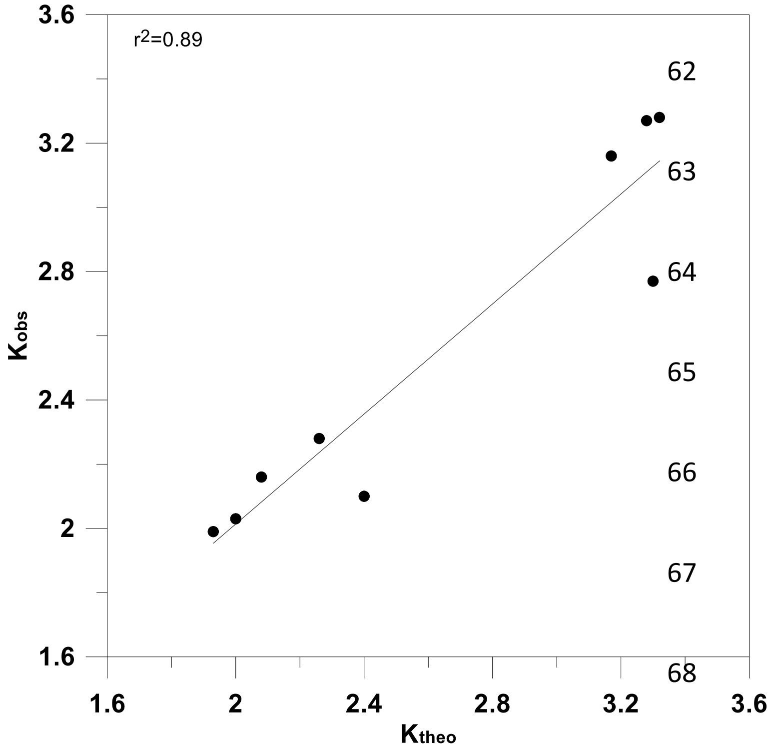

Fig. S1. k_{theo}-k_{obs} *regression and corresponding coefficient of determination (*r^2*).*

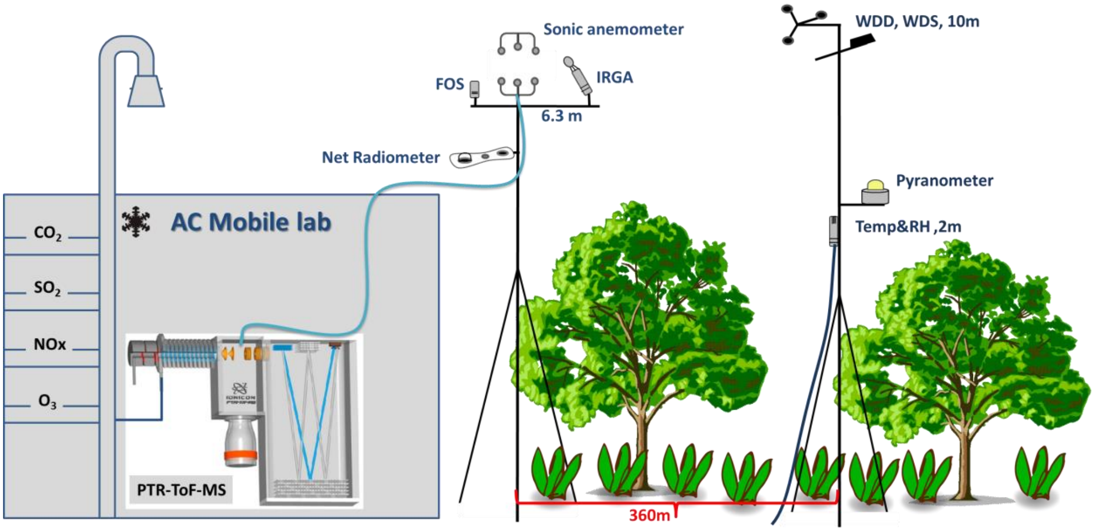

Fig. S2. *Schematic of the measurement setup. Eddy covariance measurements and open-path sensors at a height of 6.9 m were used to quantify* O_3*,* CO_2 *and* H_2O *mixing ratios, as well as VOCs by PTR-ToF-MS, which was located in an air-conditioned mobile laboratory, together with trace gas monitors. Basic meteorological parameters were measured at a distance of 360 m, within the nature park. See Sect. 2.2 in the main text for more detailed information. Note that due to technical limitations, no VOC fluxes were evaluated.*

S2. The origin of the measured VOCs

Figures S3-S8 present the average diurnal profiles of selected VOCs, suggesting a predominantly biogenic source for isoprene+2-methyl-3-buten-2-ol (MBO), monoterpenes (MTs), DMS, acetone, acetaldehyde and the sum of methyl vinyl ketone and methacrolein (MVK+MACR), which demonstrated a clear daytime increase for most of the periods (except for 14-17 September; see Sect. S6). This supports these compounds' classification as BVOCs, as determined by the analyses presented in Sects. 3.1 and 3.2 in the main text. In contrast, Figs. S3-S8 suggest that the other species, particularly H_2S, toluene and benzene, were dominated by anthropogenic sources. The correlation of the above apparent BVOCs with temperature (Fig. S10) further supports a biogenic origin for these compounds. Note that acetaldehyde and acetone, and to a lesser extent MVK+MACR, showed a somewhat less typical biogenic diurnal shape compared to the other BVOCs during some of the measurement periods. This can be explained by these species' higher solubility compared to the other BVOCs that we investigated, making them more markedly affected by drought, via stomatal activity, than the non-soluble BVOCs (Niinemets et al., 2004, 2014). This is demonstrated, for instance, for 13-14 August (see Fig. S11). This figure indicates an increase in the downward CO_2 flux after sunrise, until ~0930 h, and then a moderate decrease in this flux until ~1500 h which can be attributed to a drought-induced midday depression in the photosynthetic rate. This apparent midday depression was apparently followed by an additional increase in the photosynthetic rate at around 1600 h. Acetaldehyde and acetone showed a decrease in mixing ratios between ~0900 and 1600 h along with the decrease in CO_2's downward flux, which then peaked again at ~1600 h, suggesting their limited emission due to drought conditions. MVK+MACR did not show a peak at ~1600 h, and it was less clearly affected by the midday depression compared to acetaldehyde and acetone.

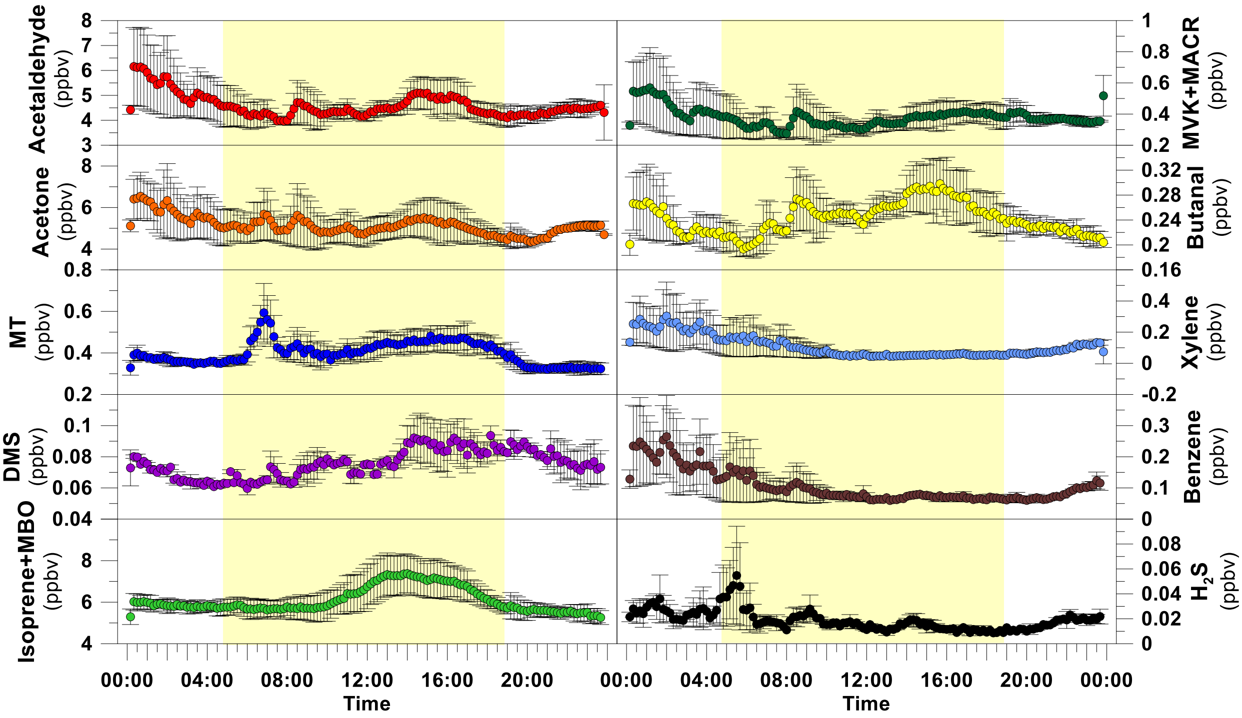

Fig. S3. *Daily average diurnal profile for selected VOCs which were dominated by biogenic sources (monoterpenes (MT), isoprene+2-methyl-3-buten-2-ol (MBO), dimethyl sulfide (DMS), acetone, acetaldehyde and the sum of methyl vinyl ketone and methacrolein (MVK+MACR)) and anthropogenic sources (butanal, xylene, benzene and* H_2S*) for* 6-7 *July (DOY 187-188) 2015. Filled circles and vertical bars represent the mean and standard deviation of the mixing ratios, respectively.*

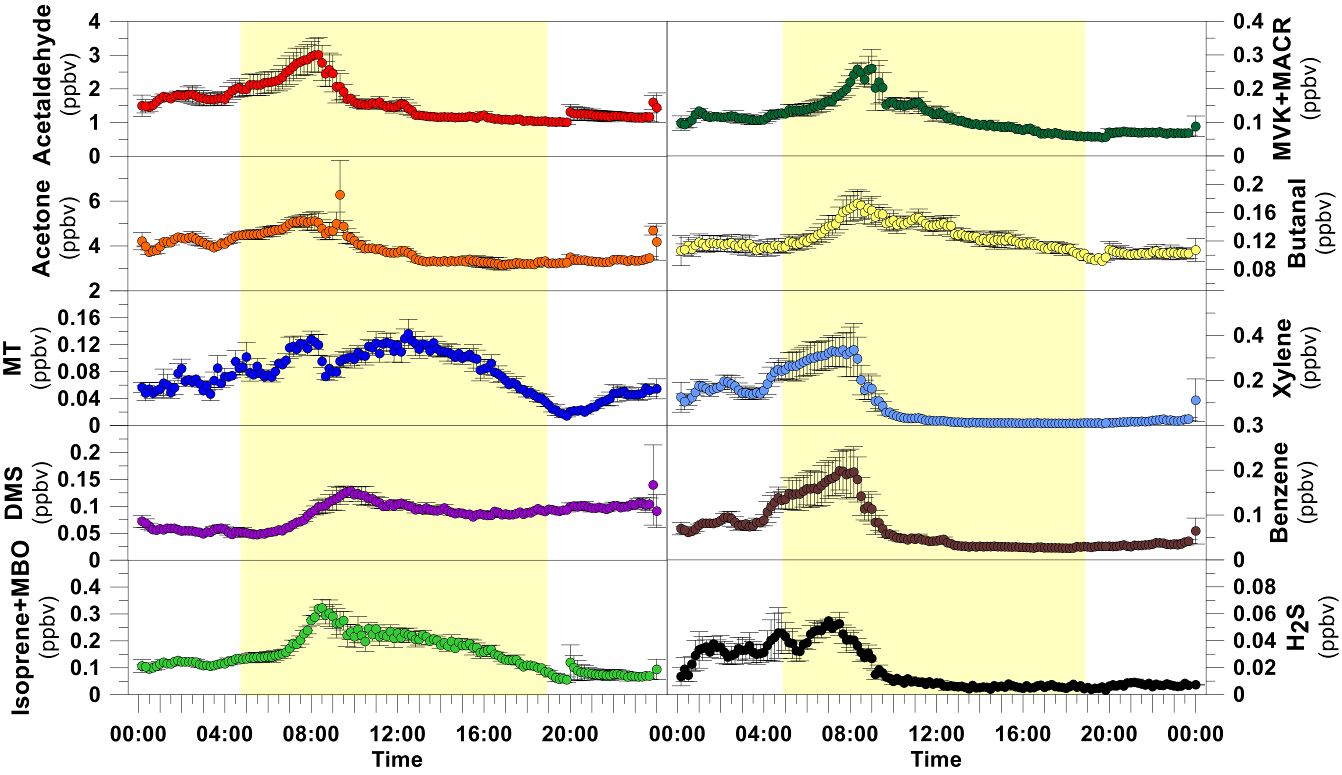

Fig. S4. *Daily average diurnal profile for selected VOCs which were dominated by biogenic sources (monoterpenes (MT), isoprene+2-methyl-3-buten-2-ol (MBO), dimethyl sulfide (DMS), acetone, acetaldehyde and the sum of methyl vinyl ketone and methacrolein (MVK+MACR)) and anthropogenic sources (butanal, xylene, benzene and* H_2S*) for 16-18 July (DOY 197-199) 2015. Filled circles and vertical bars represent the mean and standard deviation of the mixing ratios, respectively.*

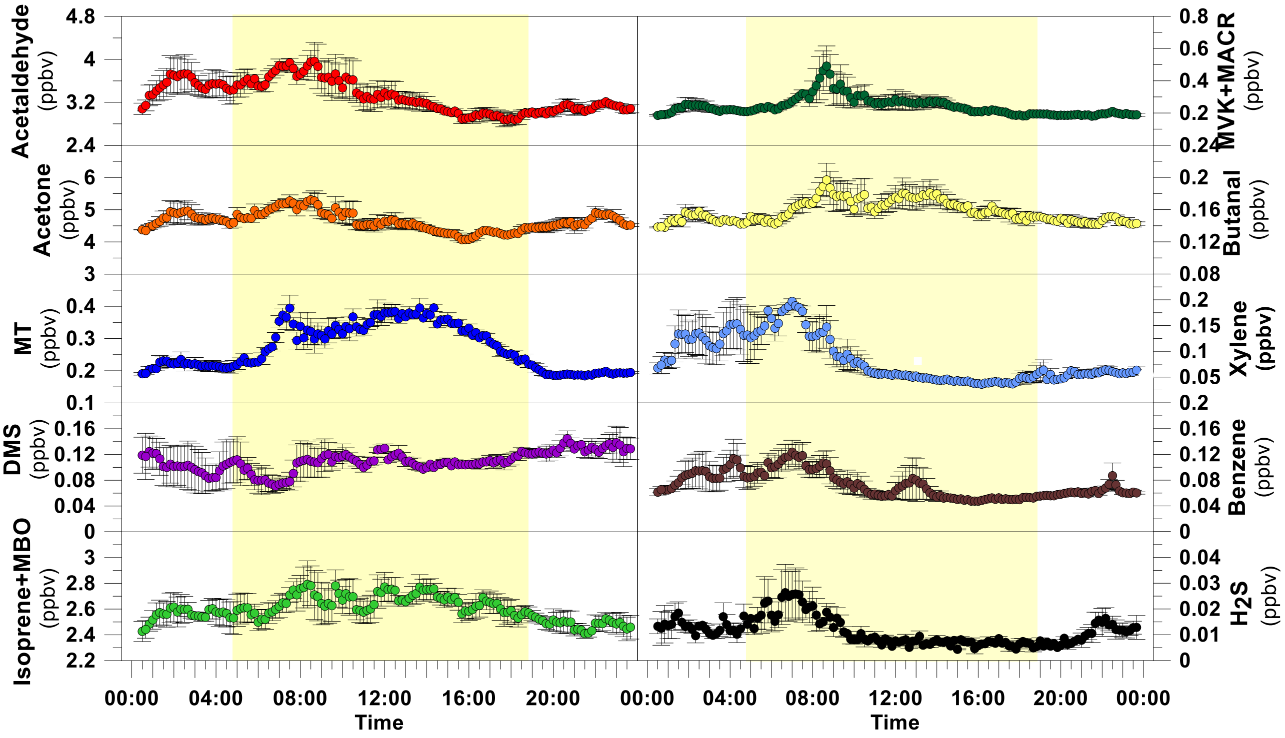

Fig. S5. *Daily average diurnal profile for selected VOCs which were dominated by biogenic sources (monoterpenes (MT), isoprene+2-methyl-3-buten-2-ol (MBO), dimethyl sulfide (DMS), acetone, acetaldehyde and the sum of methyl vinyl ketone and methacrolein (MVK+MACR)) and anthropogenic sources (butanal, xylene, benzene and* H_2S*) for 24-26 July (DOY 205-207) 2015. Filled circles and vertical bars represent the mean and standard deviation of the mixing ratios, respectively.*

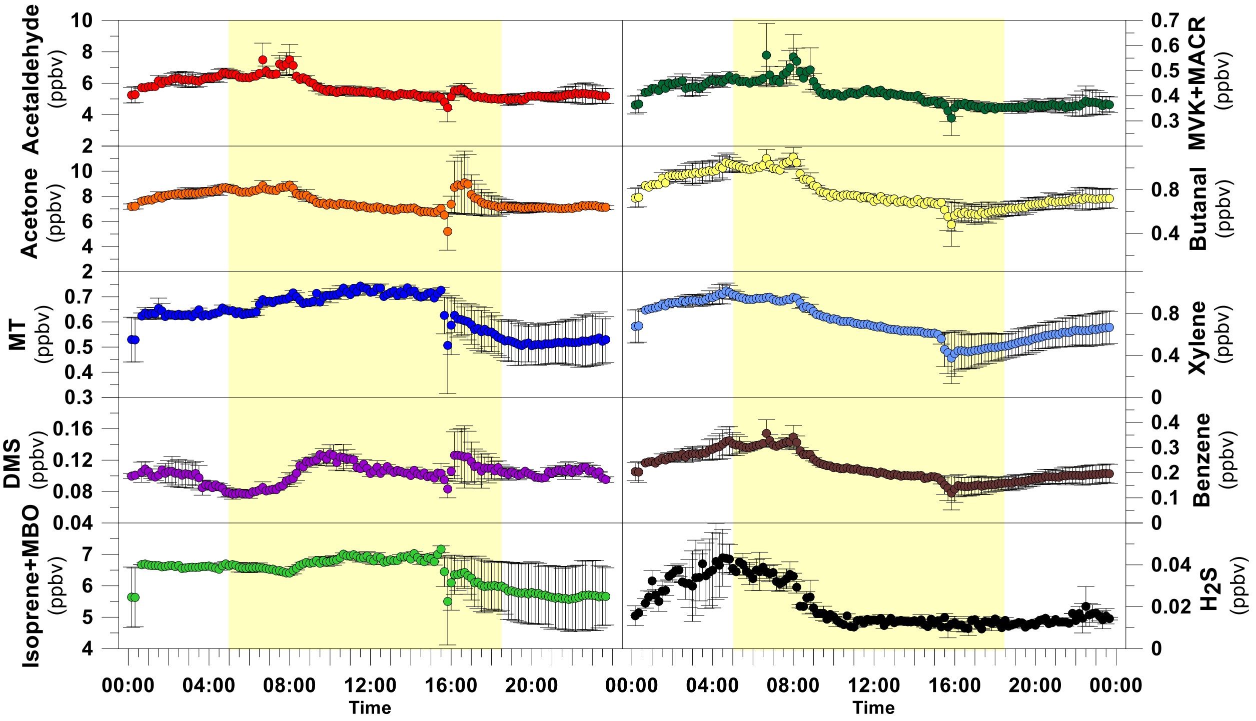

Fig. S6. *Daily average diurnal profile for selected VOCs which were dominated by biogenic sources (monoterpenes (MT), isoprene+2-methyl-3-buten-2-ol (MBO), dimethyl sulfide (DMS), acetone, acetaldehyde and the sum of methyl vinyl ketone and methacrolein (MVK+MACR)) and anthropogenic sources (butanal, xylene, benzene and* H_2S*) for 13-14* August *(DOY* 225-226*) August 2015. Filled circles and vertical bars represent the mean and standard deviation of the mixing ratios, respectively.*

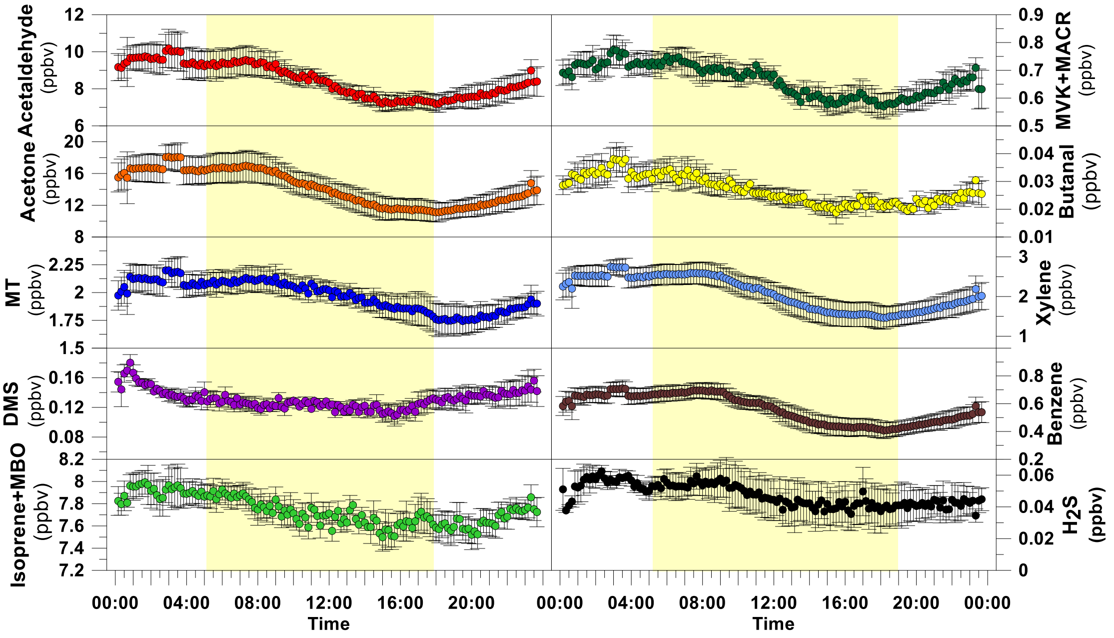

Fig. S7. *Daily average diurnal profile for selected VOCs which were dominated by biogenic sources (monoterpenes (MT), isoprene+2-methyl-3-buten-2-ol (MBO), dimethyl sulfide (DMS), acetone, acetaldehyde and the sum of methyl vinyl ketone and methacrolein (MVK+MACR)) and anthropogenic sources (butanal, xylene, benzene and* H_2S*) for 14-17 September (DOY* 257-260*) 2015. Filled circles and vertical bars represent the mean and standard deviation of the mixing ratios, respectively.*

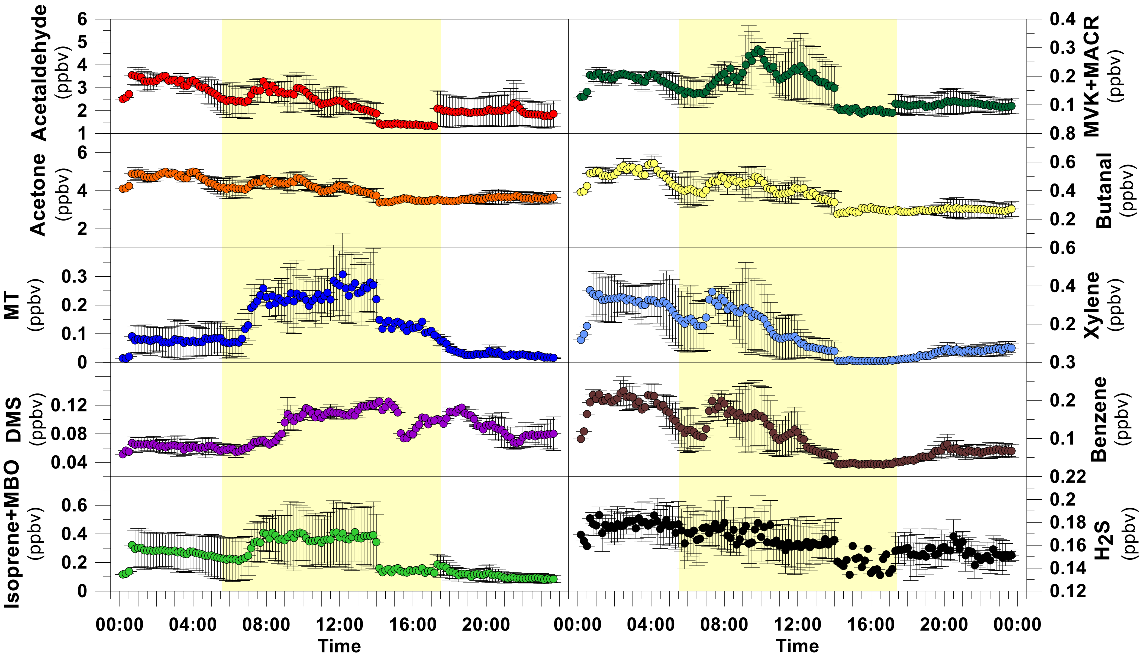

Fig. S8. *Daily average diurnal profile for selected VOCs which were dominated by biogenic sources (monoterpenes (MT), isoprene+2-methyl-3-buten-2-ol (MBO), dimethyl sulfide (DMS), acetone, acetaldehyde and the sum of methyl vinyl ketone and methacrolein (MVK+MACR)) and anthropogenic sources (butanal, xylene, benzene and* H_2S*) for* 25-26 September (268-269) *(DOY* 282-285*)* *2015. Filled circles and vertical bars represent the mean and standard deviation of the mixing ratios, respectively.*

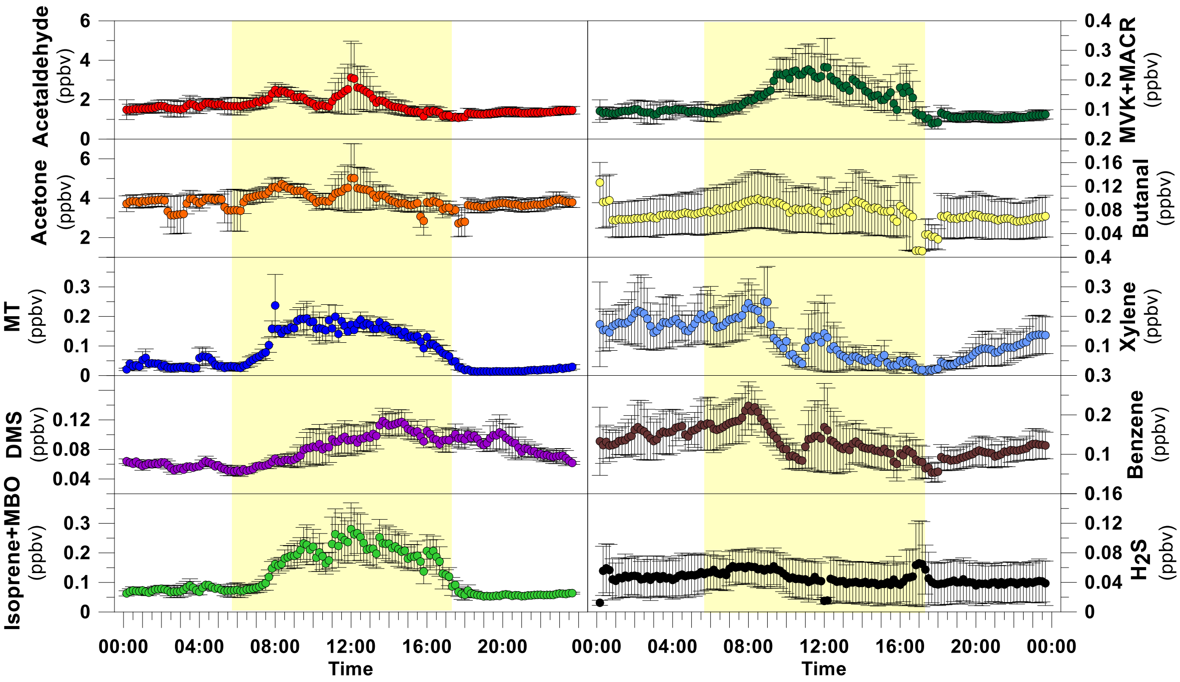

Fig. S9. *Daily average diurnal profile for selected VOCs which were dominated by biogenic sources (monoterpenes (MT), isoprene+2-methyl-3-buten-2-ol (MBO), dimethyl sulfide (DMS), acetone, acetaldehyde and the sum of methyl vinyl ketone and methacrolein (MVK+MACR)) and anthropogenic sources (butanal, xylene, benzene and* H_2S*) for 9-12 October (DOY 282-285) 2015. Filled circles and vertical bars represent the mean and standard deviation of the mixing ratios, respectively.*

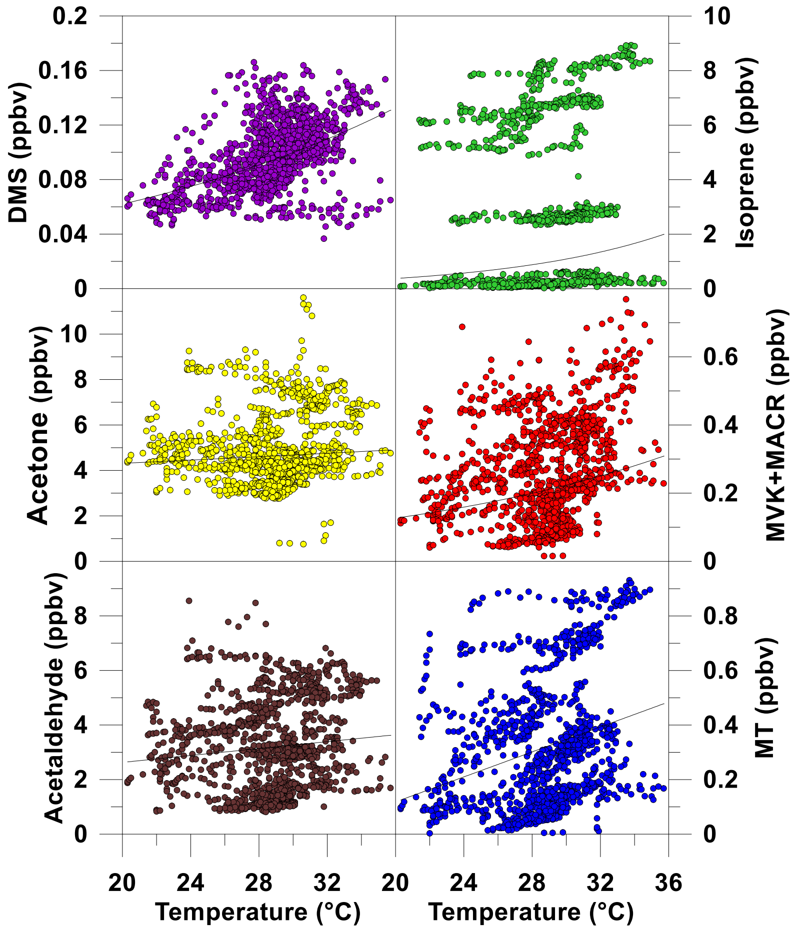

Fig. S10. *BVOC mixing ratios versus temperature. Filled circles represent mixing ratios; exponential fit lines are presented in black.*

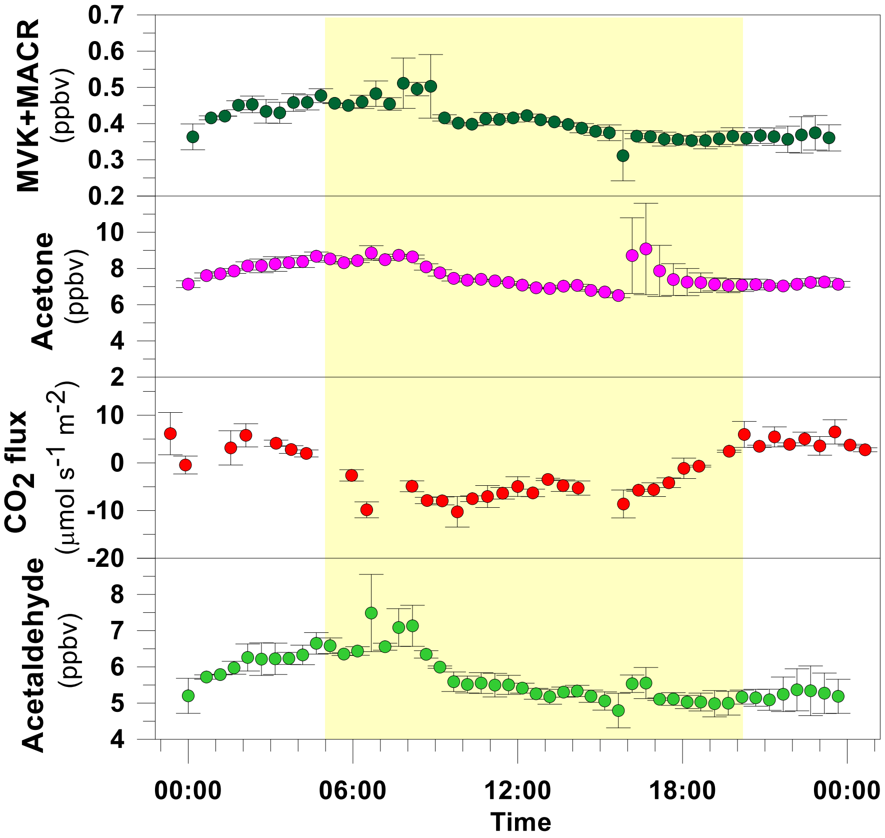

Fig. S11. *Average diurnal profile for relatively soluble BVOCs and CO_2 for 13-14 August (DOY 225-226) 2015. Filled circles and vertical bars represent the mean and standard deviation of the mixing ratios, respectively.*

S3. The origin of isoprene

The analysis in Sect. 3.2.1 in the main text indicates a biogenic origin for isoprene, primarily from the Eastern Mediterranean Sea. Figures S12-S17 present the diurnal profiles of isoprene+MBO and MT together with the diurnal profiles of acetonitrile, benzene and toluene. These figures demonstrate significantly different diurnal profiles for isoprene+MBO and MT as compared to acetonitrile, benzene and toluene, with a clear increase in mixing ratios during the day for the first two, except for 14-17 September (see Sect. S6). Hence, these figures reinforce the lack of a significant anthropogenic contribution from the two highways which are located to the west of the measurement site, considering that acetonitrile, benzene and toluene can be used as proxies for traffic emission. Note that a correlation of acetonitrile with acetone and acetaldehyde suggests that the former is probably also emitted from a biogenic source. This was most clear for 13-14 August (see Fig. S18). Figure S19 presents a comparison between the diurnal profile of carbon monoxide (CO) and isoprene+MBO for 13 August, the only day for which CO measurements were available. This figure also reinforces the lack of a significant anthropogenic contribution from the two highways, as CO is used as a proxy for traffic emission.

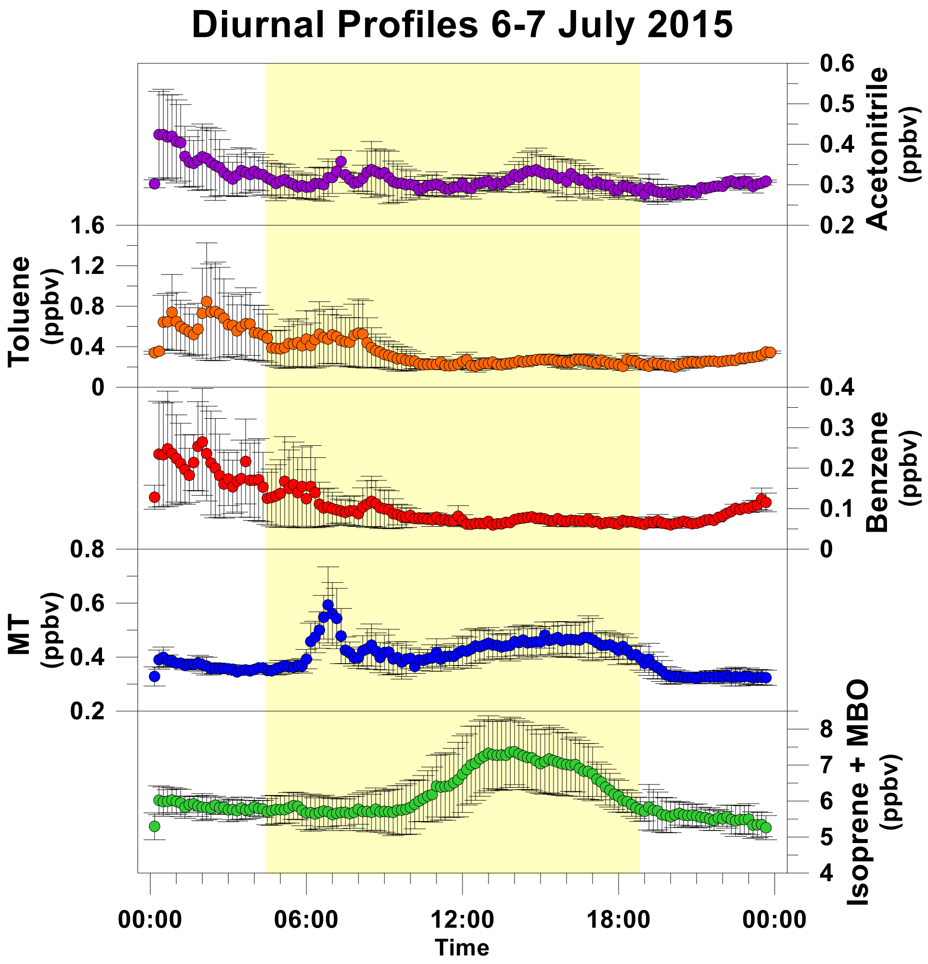

Fig. S12. *Average diurnal profile for isoprene+MBO, monoterpenes (MT), benzene, toluene and acetonitrile for 6-7 July 2015. Filled circles and vertical bars represent the mean and standard deviation of the mixing ratios, respectively.*

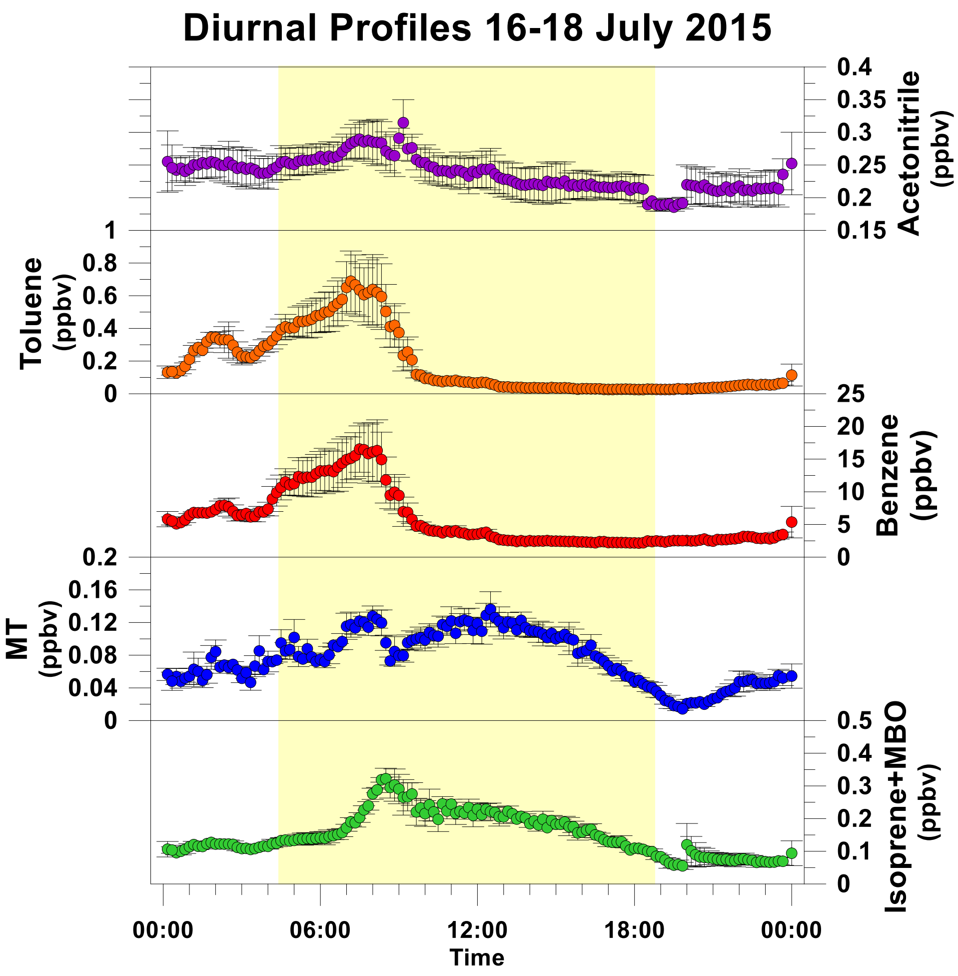

Fig. S13. *Average diurnal profile for isoprene+MBO, monoterpenes (MT), benzene, toluene and acetonitrile for 16-18 July 2015. Filled circles and vertical bars represent the mean and standard deviation of the mixing ratios, respectively.*

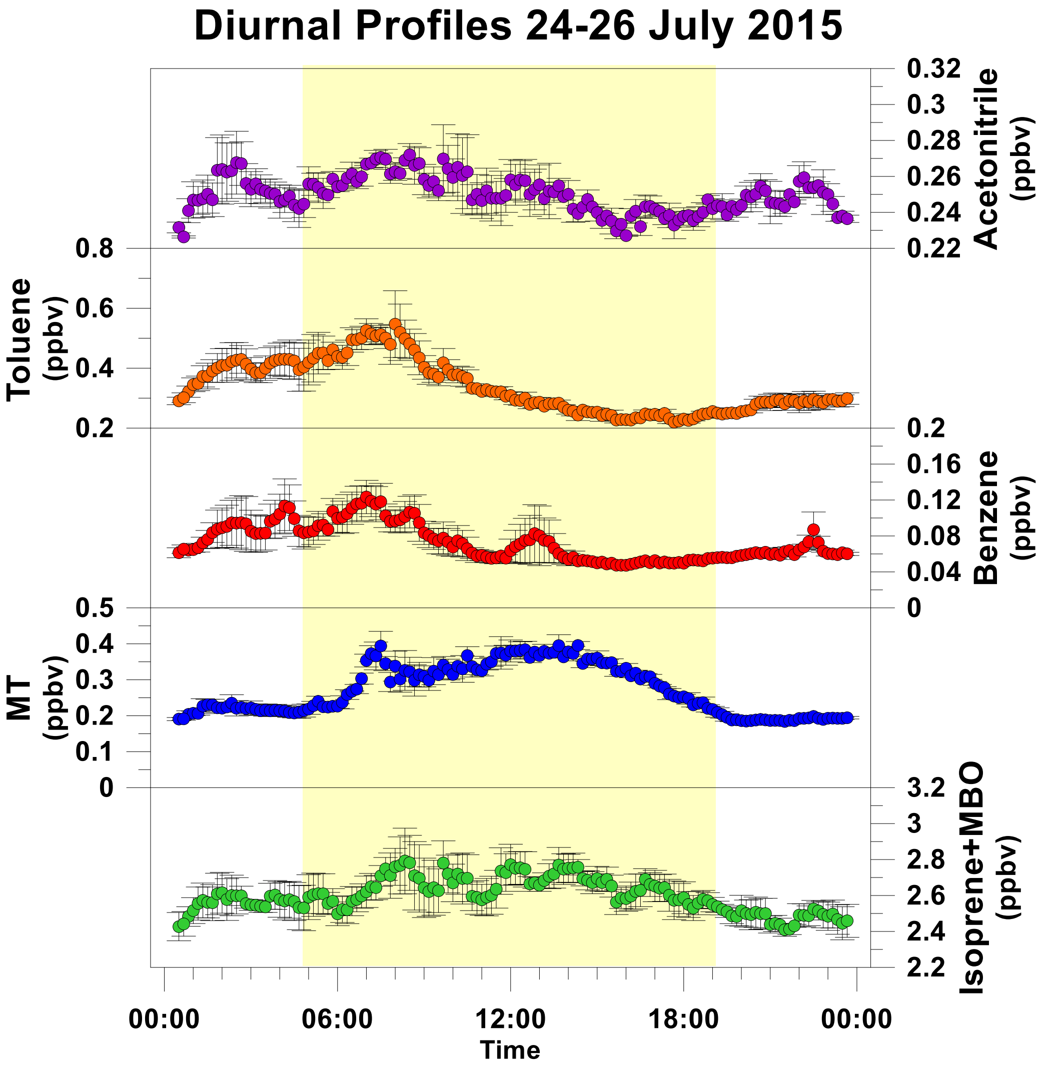

Fig. S14. *Average diurnal profile for isoprene+MBO, monoterpenes (MT), benzene, toluene and acetonitrile for 24-26 July 2015. Filled circles and vertical bars represent the mean and standard deviation of the mixing ratios, respectively.*

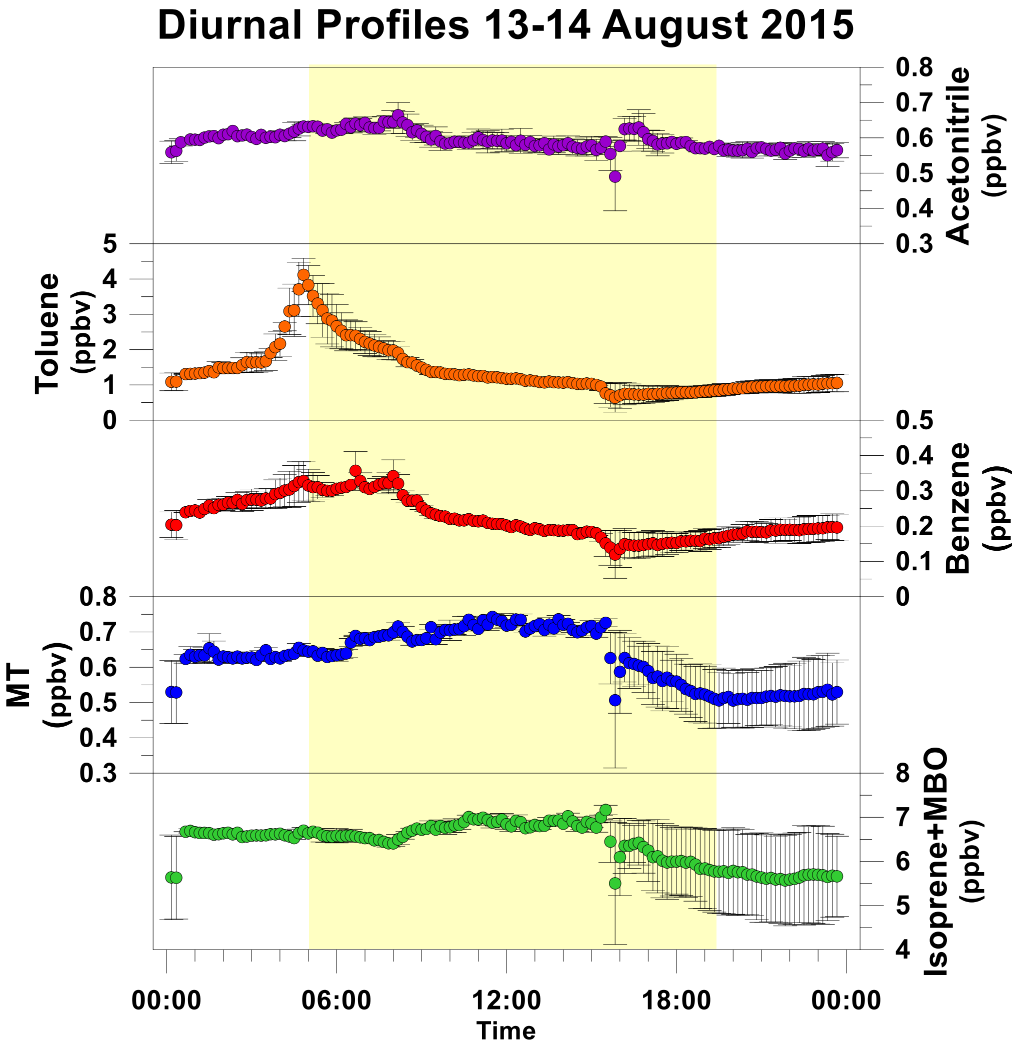

Fig. S15. *Average diurnal profile for isoprene+MBO, monoterpenes (MT), benzene, toluene and acetonitrile for 13-14 August 2015. Filled circles and vertical bars represent the mean and standard deviation of the mixing ratios, respectively.*

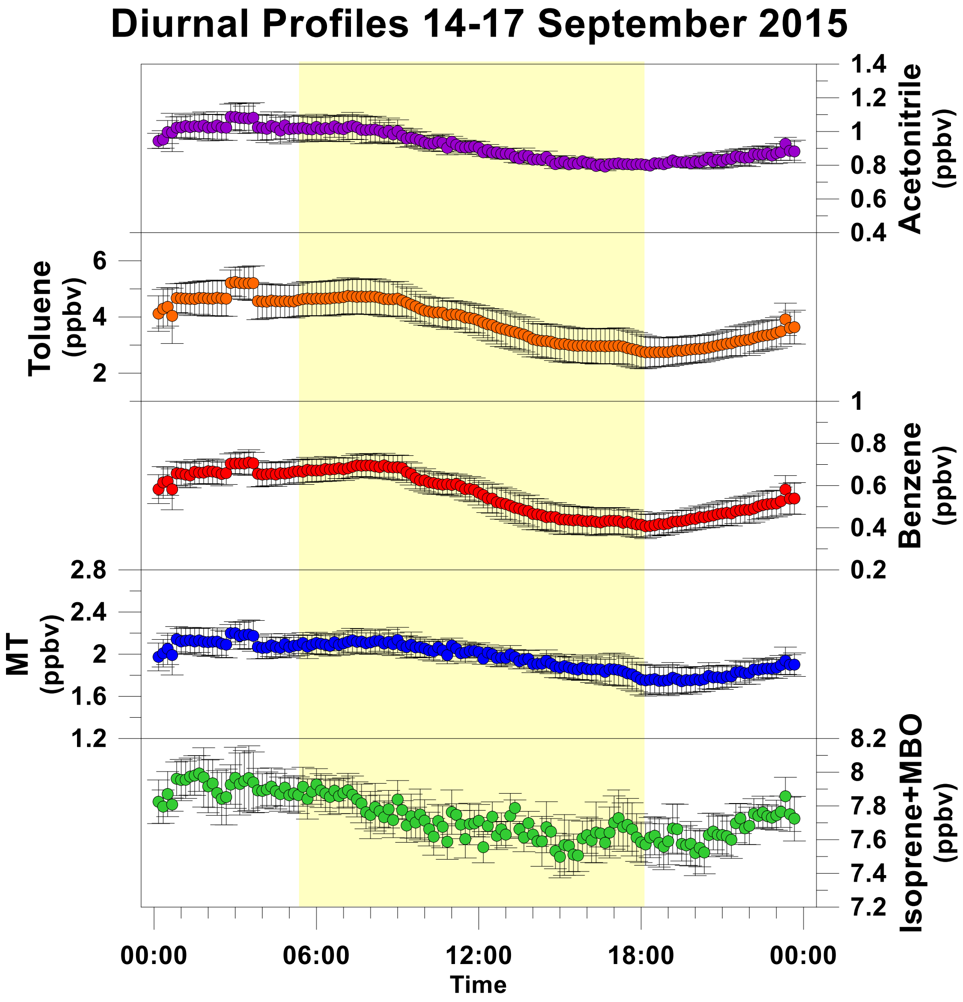

Fig. S16. *Average diurnal profile for isoprene+MBO, monoterpenes (MT), benzene, toluene and acetonitrile for 14-17 September 2015. Filled circles and vertical bars represent the mean and standard deviation of the mixing ratios, respectively.*

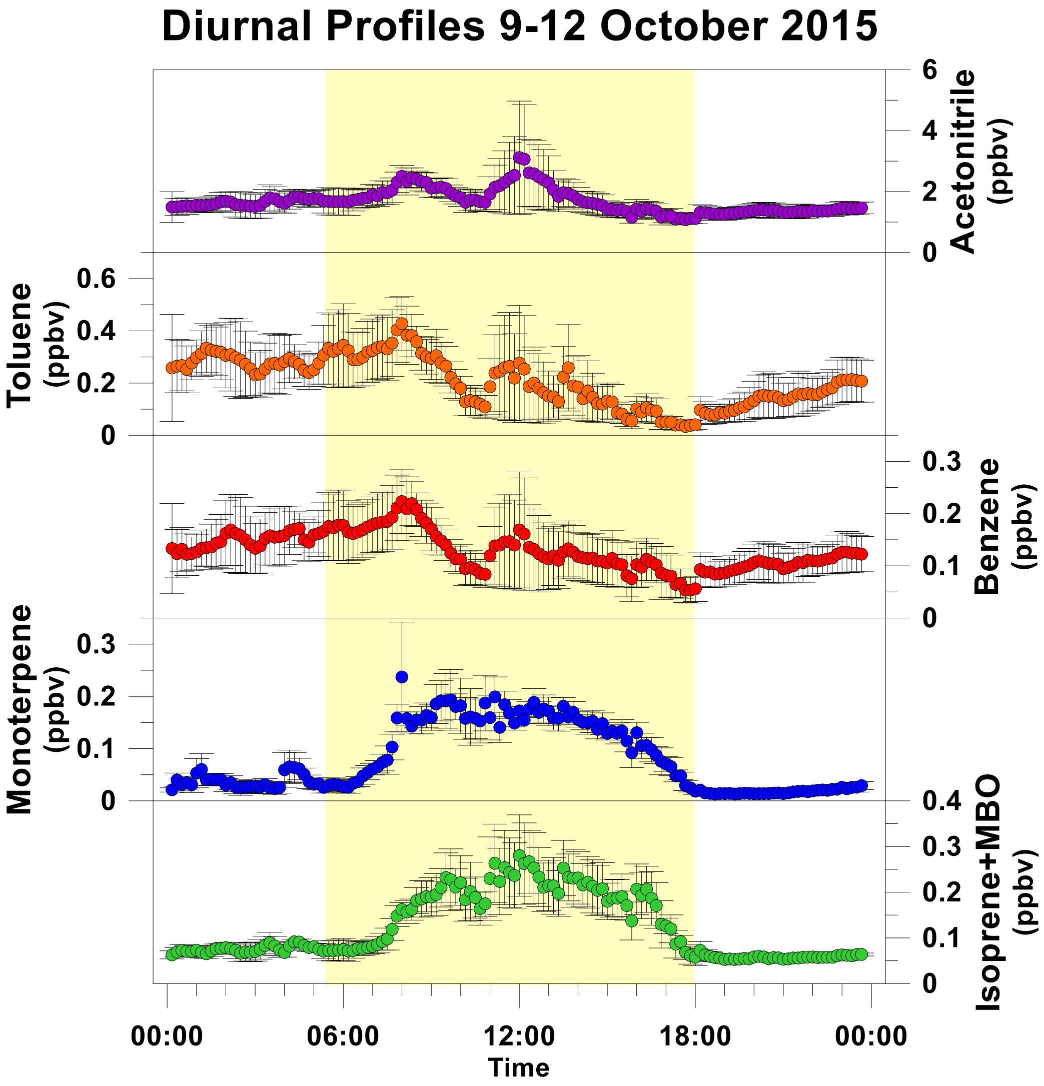

Fig. S17. *Average diurnal profile for isoprene+MBO, monoterpenes (MT), benzene, toluene and acetonitrile for 9-12 October 2015. Filled circles and vertical bars represent the mean and standard deviation of the mixing ratios, respectively.*

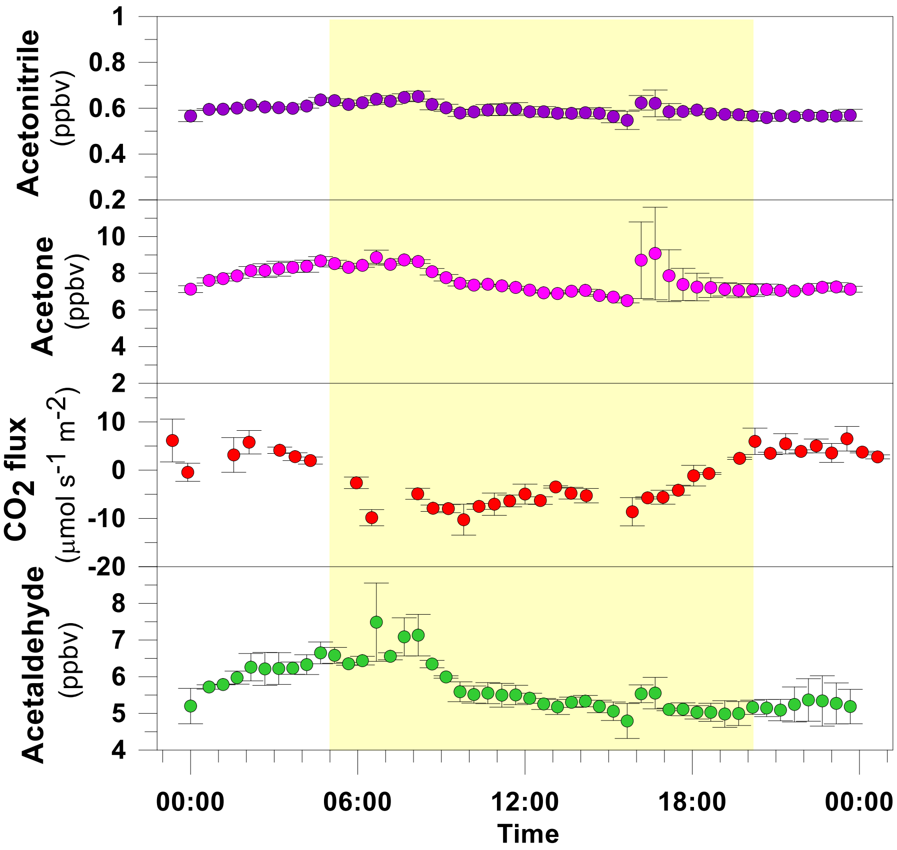

Fig. S18. *Average diurnal profile for acetonitrile, acetone and acetaldehyde mixing ratios and CO_2 flux during 13-14 August 2015 (DOY 225-226). Filled circles and vertical bars represent the mean and standard deviation of the mixing ratios, respectively.*

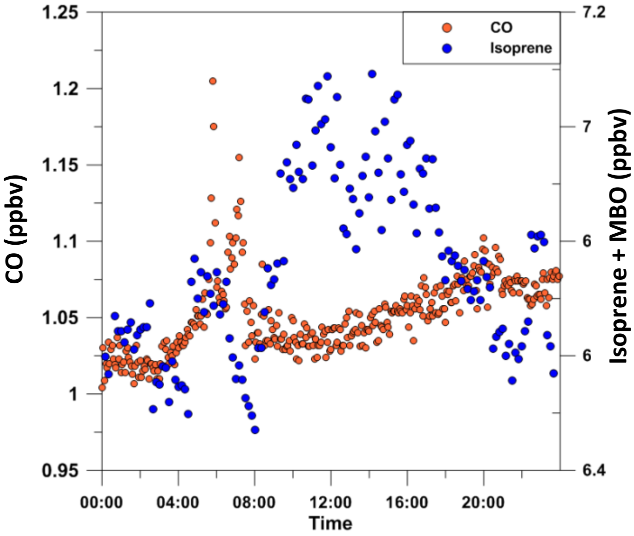

Fig. S19. *Comparison between CO and isoprene+MBO profiles on 13 August 2015.*

The discussion in Sect. 3.2.1 of the main text refers to high day-to-day variations in isoprene+MBO compared to most of the BVOCs, while its mixing ratios ranged from 0.03 ppbv to nearly 9 ppbv. Table S3 compares the day-to-day variation of the investigated BVOCs. The table indicates higher day-to-day variations for isoprene compared to the other investigated BVOCs.

Table S3. Coefficients of variation based on the daily mean mixing ratios of the investigated BVOCs

BVOC	**Standard deviation of the daily mean mixing ratios (ppbv)**	**Coefficient of variation**
Isoprene	2.914	1.138
Acetaldehyde	1.539	0.549
Acetone	1.339	0.321
Monoterpene	0.227	0.908
MVK+MACR	0.130	0.650
DMS	0.014	0.323

Fig. S20 demonstrates high isoprene+MBO mixing ratios in case when air masses were transported over the Eastern Mediterranean Sea, but not over the aquafarms. This, in addition to the robustness of the isoprene+MBO mixing ratios with respect to the specific wind direction, reinforces a major contribution of the Mediterranean Sea to isoprene emissions (see Sect. 3.2.1 in the main text).

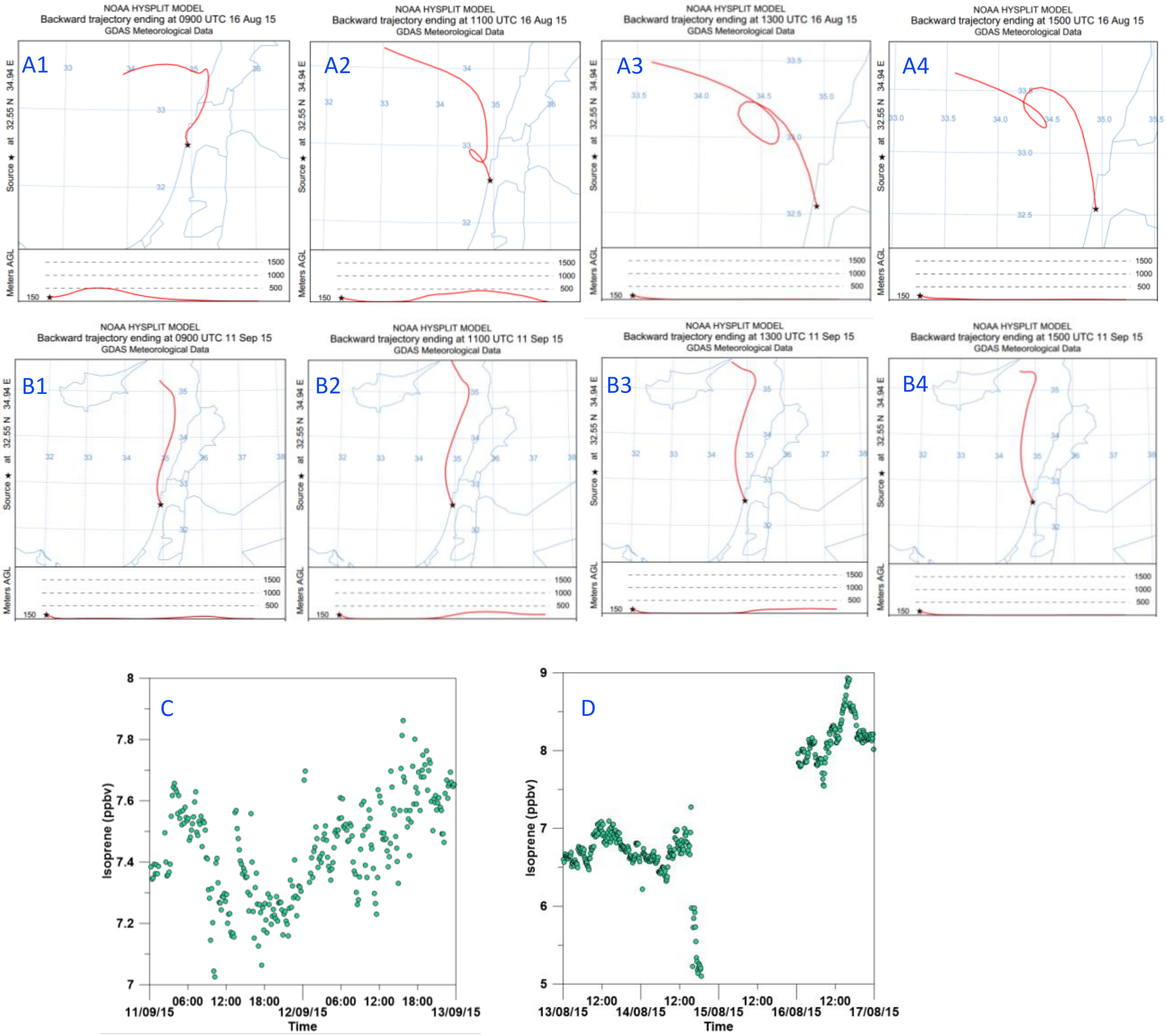

Figure S20. *Backward trajectories for 16 August 2015 (A), and 11 September 2015 (B), for the hours 0900 (A1, B1), 1100 (A2, B2), 1300 (A3, B3), 1500 (A4, B4). Isoprene+MBO time series for 11–12 September 2015 (C) and 13–16 August 2015*

(D). This example is used to demonstrate high isoprene+MBO mixing ratios when the trajectories pass only over the Mediterranean Sea, and not over the aquafarms.

Figure S21 presents a scatter plot of MBO* (m87/m69 >13%; see Sect. 3.2.1 in the main text) mixing ratios vs. temperature for the six measurement periods, to complement Figs. 5 and 7 in the main text which show the same analysis for isoprene+MBO and isoprene (m87/m69<13%). Figure S21 demonstrates a weaker association between MBO* and temperature compared to isoprene (see Fig. 6 in the main text).

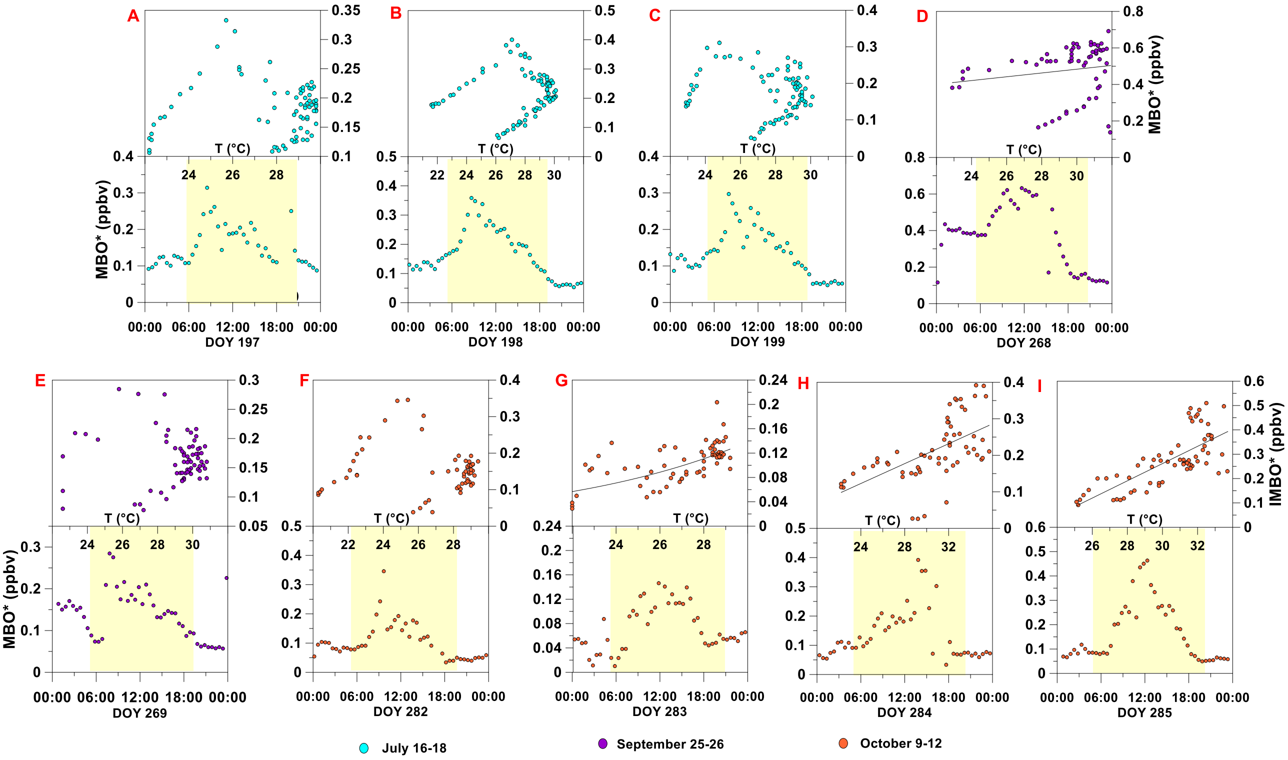

Fig. S21. *Diurnal average of MBO* (m87/m69>13%) mixing ratios and dependence on temperature (T). Upper panels show regression between measured m87/m69 >13% and T and lower panels show mixing ratios for m87/m96>13%. Yellow shaded area represents daylight hours.*

S4. Origin of MVK+MACR from the memorial garden

Figure 3 in the main text indicates elevated emission of MVK+MACR—isoprene oxidation products—from both the west and southeast. The former can be attributed to isoprene originating from the sea (Sect. 3.2.1 in the main text), while the latter could suggest emission of isoprene from the memorial garden. Considering the distance of the memorial garden (~40-400 m) and the resulting transport time to the measurement site under typical daytime measured wind speed (3.5 m s^{-1}), about 0.5-5% of the isoprene could be oxidized assuming an isoprene lifetime of ~37 min (see Sect. 2.2.1 in the main text). Our measurements indicated that MVK+MACR mixing ratios reach about 5-9% of the isoprene+MBO mixing ratios. Hence, considering that most of the daytime measured isoprene+MBO contribution from this direction can probably be attributed to MBO (Fig. 5B vs. Fig. 4 in the main text), we do not expect a significant contribution of isoprene oxidation to the observed MVK+MACR. To some extent, the apparent elevated contribution to MVK+MACR from the memorial garden can be attributed to 2-hydroxy-2-methylpropanal (HMPR), a major OH-induced MBO-oxidation product (Kaser et al., 2013 and references therein). Vegetation thinning is an additional potential source for both MVK and MACR (Brilli et al., 2014).

S5. MEGAN v2.1 results

Table S4 provides the fractional contribution of MTs from the vegetation at Ramat Hanadiv as predicted by the MEGAN v2.1 simulations, to complement the discussion in Sect. 3.2.2 in the main text.

Table S4. Emission rates evaluated by MEGAN v2.1

	MT*	Acetone	Acetaldehyde	MBO	DMS
Average $\left(\frac{\mu g}{m^2 \cdot h}\right)$	58.62	16.363	10.629	10.248	0.477
Range $\left(\frac{\mu g}{m^2 \cdot h}\right)$	131.491	28.021	41.462	46.932	0.817

**MT: several key MTs are expected to be emitted from the nature park (see Sect. 2.1 in the main text), increasing in emission rate according to: myrcene (2%) > t-beta-ocimene (6%) > 3-carene (15%) > limonene (16%)> β-pinene (19%) > α-pinene (27%), and other MTs contributing 14%.*

Table S5. Contribution of specific species to monoterpene (MT) emissions based on MEGAN v2.1 simulations

Species	***Quercus calliprinos***	***Pistacia lentiscus***	***Rhamnus lycioides***	***Pinus halepensis***	***Phillyrea latifolia***	***Cupressus***	***Sarcopoterium spinosum***	***Calicotome villosa***
Fraction (%)	**48.1**	**19.8**	**0.36**	**14.0**	**7.12**	**6.17**	**2.36**	**2.12**

S6. Elevated mixing ratios and irregular BVOC diurnal profiles for DOY 257-260

During DOY 257-260, we measured somewhat elevated mixing ratios for several VOCs (Fig. 2 in the main text). Because this period was much hazier than the other investigated periods and characterized by low solar radiation intensity (see Fig. S22), we hypothesized that the high mixing ratios were induced to some extent by a smaller than usual boundary layer height (BLH) via reduction of atmospheric instability.

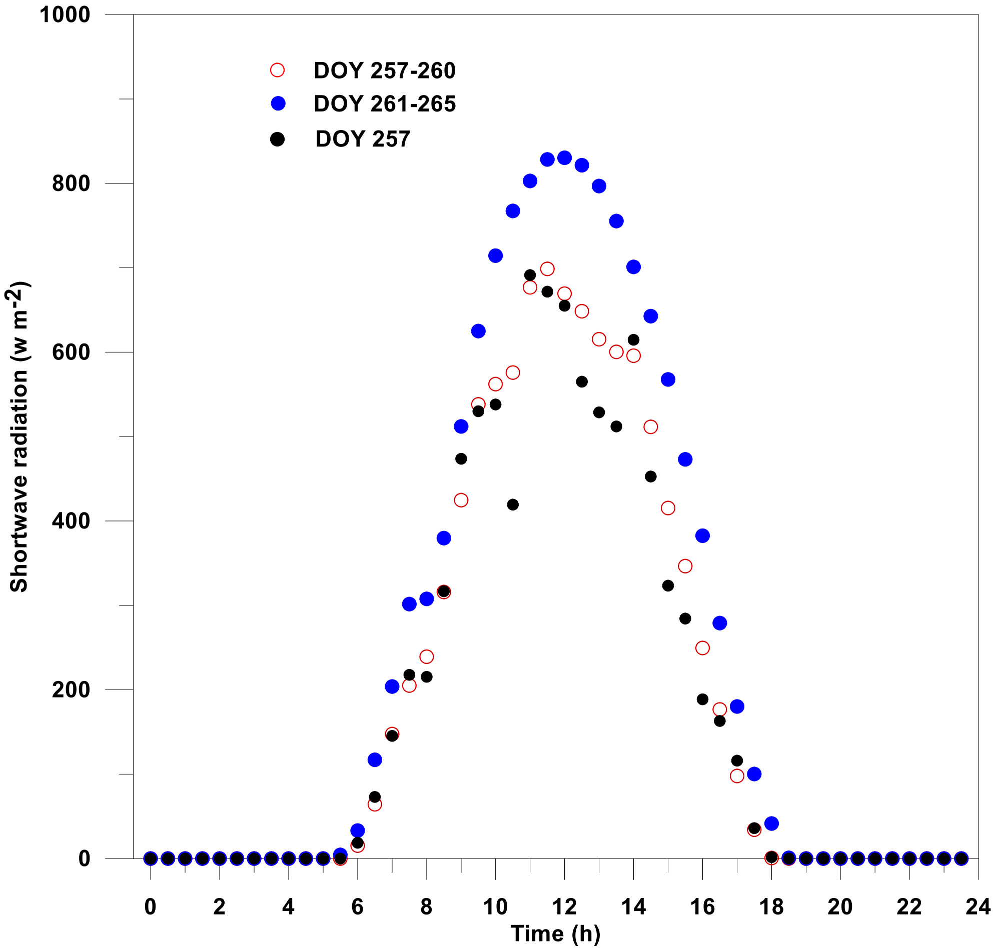

Fig. S22. *Comparison of average diurnal profiles of downward shortwave solar radiation during DOY 257-260, DOY 262-265 and DOY 257. Note that due to lack of shortwave solar radiation during DOY 257–265, the presented profiles were reconstructed from a satellite dataset (NCEP/DOE AMIP-II Reanalysis (Reanalysis-2) and in-situ global solar radiation measurements.*

To investigate this hypothesis, we ran the mesoscale weather research and forecasting (WRF) model, version 3.7.1. A detailed description of the model can be found at http://www.wrfmodel.org/index.php. A 1-km horizontal spacing domain was used with 190 × 529 grid points in the west–east and south–north directions, respectively, covering the whole area of Israel, as shown in Fig. S23.

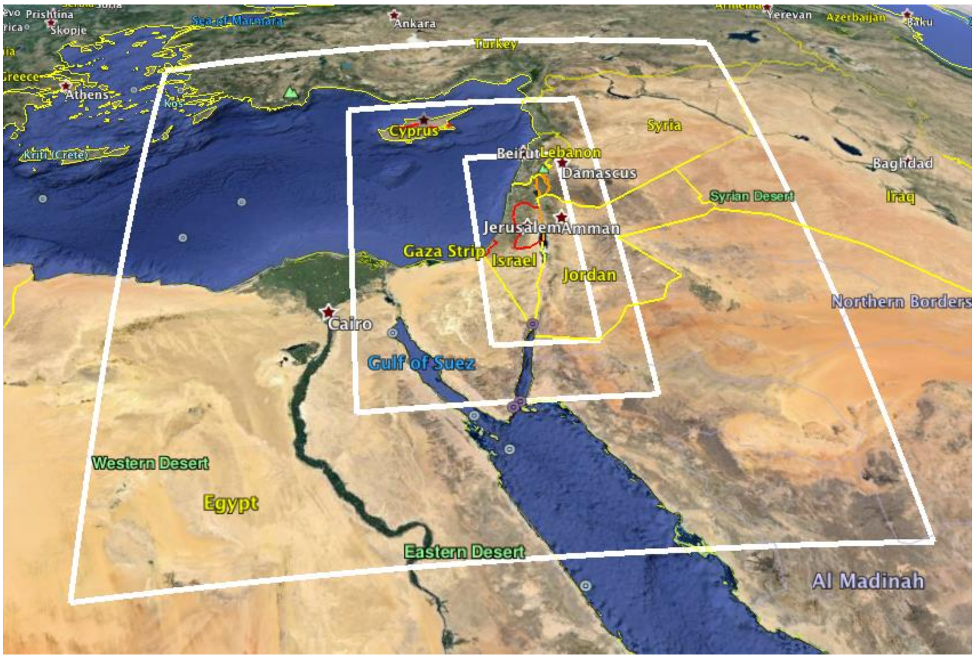

Fig. S23. *Map of the three nested domain grids of WRF simulations in the Eastern Mediterranean (domain resolution: Domain 1 = 9 km, Domain 2 = 3 km, Domain 3 = 1 km). The WRF domain covers areas in southern Lebanon, Israel, West Syria, West Jordan, and South Egypt. Background imagery from © Google Earth.*

The 1-km resolution constitutes a compromise between optimal representation of the terrain and land use, suitability of the planetary boundary layer (PBL) parameterizations in the WRF model and computational requirements. The vertical grid included 30 levels within the first 1 km above the ground. Initial and boundary conditions were provided by NCEP GFS analysis (https://rda.ucar.edu/datasets/ds083.2/), which has six hourly time resolutions and $0.25^{o} \times 0.25^{o}$ horizontal resolution. The high vertical and horizontal resolution enabled us to capture the local effect of terrain on meteorology.

The model simulations indicated that the BLH for DOY 257 was smaller by ~23.2% than the average for September (see Fig. S25), but not for DOY 258-260. The diurnal profiles of the BVOCs for the period of DOY 257-260, however, differed significantly from other periods, by not showing any clear increase during the daytime, and starting to continuously decrease from about 0800-0900 h, except for DMS for which the decrease started earlier (see Fig. S24). One explanation for this may be the lower solar radiation and its more moderate increase before noontime compared to the other investigated periods (see Fig. S22), together with expansion of the BLH before noontime (see Fig S25). Another explanation is a subsidence of air from the upper troposphere which is typical for the studied area during the summer, leading to a significant change in mixing ratios, such as of O_3, within the boundary layer (e.g., Tyrlis and Lelieveld, 2013; Zanis et al., 2014). Such subsidence can frequently lead to shallowing of the BLH. As is evident from our model simulations, DOY 257-260 were characterized by notably early (~1000 h) shallowing of the BLH compared to the other measurement period (DOY 268-269), strongly supporting the occurrence of subsidence for DOY 257-260.

The fact that anthropogenic trace gases showed similar diurnal profiles to those of the BVOCs, but with an earlier decrease in mixing ratios during the morning (Fig. S24), suggests that the former were also significantly affected by the subsidence, while the delayed and more moderate decrease for BVOCs was due to an increase in emission with increasing temperature and radiation intensity. Our analysis is insufficient to conclusively account for the elevated BVOC mixing ratios and irregular diurnal profiles during DOY 257-260. However, we excluded this period from the rest of the analyses (except for Fig. 2 in the main text) due to the irregular diurnal profiles for BVOCs during this period.

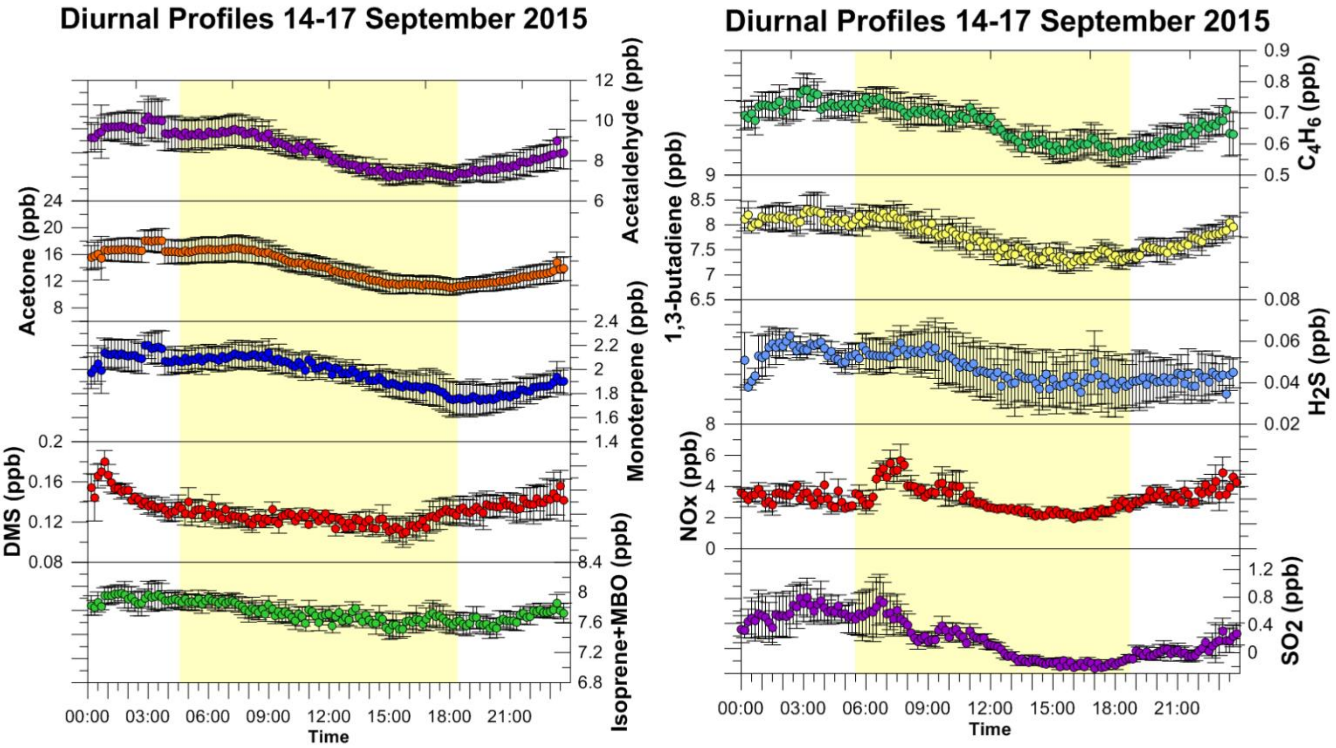

Figure S24. Average diurnal profiles of BVOCs (A) and anthropogenic trace gases (B) for 14-17 September 2015.

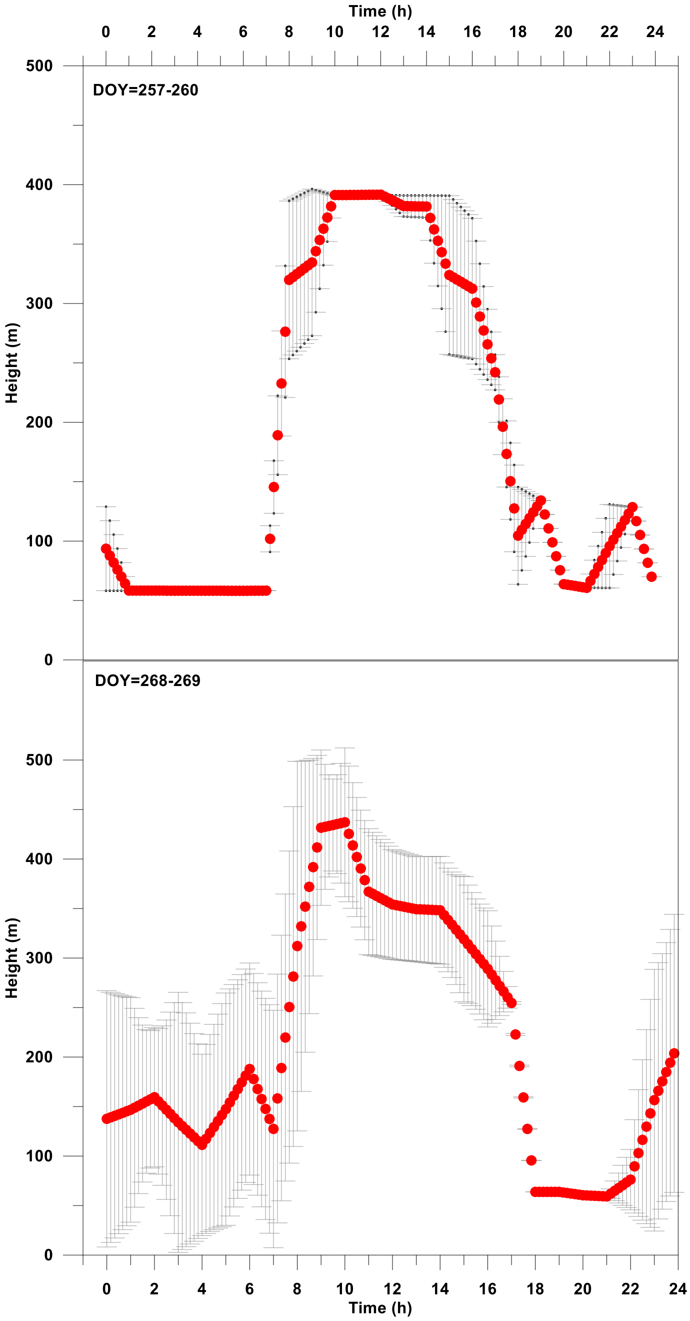

Fig. S25. Average diurnal profile of the boundary layer height (BLH) during DOY 257-260 (upper panel) and DOY 268-269 (lower panel). Gray vertical error bars represent standard deviation.

S7. Emission of green leaf volatiles (GLVs) from the memorial garden

Our analysis indicated elevated mixing ratios of wounded species' emissions from the memorial garden, where frequent thinning is performed (Sect. 3.2 in the main text).

Figure S25 shows the potential sources of GLVs, including methanol (m/z=33.034), hexanal (m/z=83.085) and hexenal (m/z=57.033 and m/z=99.080). For each wind sector, the percentage of time corresponding to several mixing-ratio ranges is presented, individually for each species. Note that hexenal is also detected at m/z=43.018 and m/z=81.080 (Brilli et al., 2011; Pang, 2015), but we did not include these fragments in the hexenal mixing ratios because m/z=43.018 can be affected by 1-hexyl acetate and other GLV fragments (m/z=43.018), while m/z=81.080 can be affected by MTs. Hexanal is also detected at m/z=83.085 and m/z=101.096, but we used only m/z=83.085 to evaluate hexanal mixing ratios, considering that it contributed about 99% to the mixing ratios. Fig. S26 indicates elevated emission of GLVs, but comparison of this figure with Fig. 4 in the main text suggests that there was no clearly higher excess of these GLVs from the southeast, compared to the other wounding BVOCs.

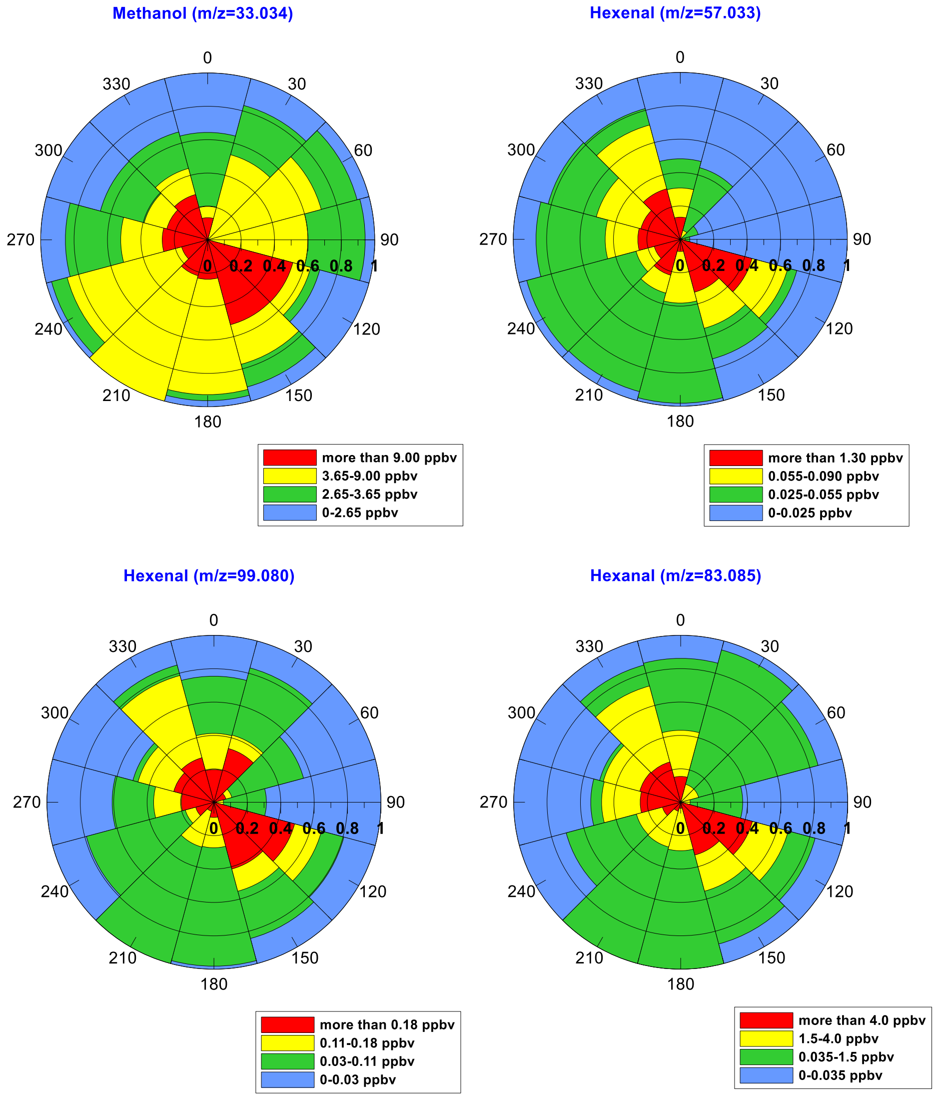

Fig. S26. Methanol, hexanal and hexenal mixing ratios as a function of the contribution from each wind sector. The radial dimension represents the fraction of time for each wind sector during which the mixing ratios were within a certain range, as specified in the color key.

References

Brilli, F., Ruuskanen, T. M., Schnitzhofer, R., Müller, M., Breitenlechner, M., Bittner, V., Wohlfahrt, G., Loreto, F. and Hansel, A.: Detection of plant volatiles after leaf wounding and darkening by proton transfer reaction “time-of-flight” mass spectrometry (ptr-tof), PLoS One, 6(5), doi:10.1371/journal.pone.0020419, 2011.

Brilli, F., Gioli, B., Zona, D., Pallozzi, E., Zenone, T., Fratini, G., Calfapietra, C., Loreto, F., Janssens, I. A. and Ceulemans, R.: Simultaneous leaf- and ecosystem-level fluxes of volatile organic compounds from a poplar-based SRC plantation, Agric. For. Meteorol., 187, 22–35, doi:10.1016/j.agrformet.2013.11.006, 2014.

Cappellin, L., Karl, T., Probst, M., Ismailova, O., Winkler, P. M., Soukoulis, C., Aprea, E., Märk, T. D., Gasperi, F. and Biasioli, F.: On quantitative determination of volatile organic compound concentrations using proton transfer reaction time-of-flight mass spectrometry, Environ. Sci. Technol., 46(4), 2283–2290, doi:10.1021/es203985t, 2012.

de Gouw, J. A., Goldan, P. D., Warneke, C., Kuster, W. C., Roberts, J. M., Marchewka, M., Bertman, S. B., Pszenny, A. A. P. and Keene, W. C.: Validation of proton transfer reaction-mass spectrometry (PTR-MS) measurements of gas-phase organic compounds in the atmosphere during the New England Air Quality Study (NEAQS) in 2002, J. Geophys. Res. Atmos., 108(D21), doi:10.1029/2003JD003863, 2003.

de Gouw, J. and Warneke, C.: Measurements of volatile organic compounds in the earth’s atmosphere using proton-transfer-reaction mass spectrometry, Mass Spectrom. Rev., 26(2), 223–257, doi:10.1002/mas.20119, 2007.

Kaser, L., Karl, T., Schnitzhofer, R., Graus, M., Herdlinger-Blatt, I. S., DiGangi, J. P., Sive, B., Turnipseed, A., Hornbrook, R. S., Zheng, W., Flocke, F. M., Guenther, A., Keutsch, F. N., Apel, E. and Hansel, A.: Comparison of different real time VOC measurement techniques in a ponderosa pine forest, Atmos. Chem. Phys., 13(5), 2893–2906, doi:10.5194/acp-13-2893-2013, 2013.

Lindinger, W., Hansel, A. and Jordan, A.: On-line monitoring of volatile organic compounds at pptv levels by means of Proton-Transfer-Reaction Mass Spectrometry (PTR-MS) Medical applications, food control and environmental research, Int. J. Mass Spectrom. Ion Process., 173(3), 191–241, doi:10.1016/s0168-1176(97)00281-4, 1998.

Niinemets, Ü., Loreto, F. and Reichstein, M.: Physiological and physicochemical controls on foliar volatile organic compound emissions, Trends Plant Sci., 9(4), 180–186, doi:10.1016/j.tplants.2004.02.006, 2004.

Niinemets, Ü., Fares, S., Harley, P. and Jardine, K. J.: Bidirectional exchange of biogenic volatiles with vegetation: Emission sources, reactions, breakdown and deposition, Plant, Cell Environ., 37(8), 1790–1809, doi:10.1111/pce.12322, 2014.

Pang, X.: Biogenic volatile organic compound analyses by PTR-TOF-MS: Calibration, humidity effect and reduced electric field dependency, J. Environ. Sci. (China), doi:10.1016/j.jes.2015.01.013, 2015.

Tyrlis, E. and Lelieveld, J.: Climatology and dynamics of the summer Etesian winds over the eastern Mediterranean, J. Atmos. Sci., 70(11), 3374–3396, doi:10.1175/JAS-D-13-035.1, 2013.

Zanis, P., Hadjinicolaou, P., Pozzer, A., Tyrlis, E., Dafka, S., Mihalopoulos, N. and Lelieveld, J.: Summertime free-tropospheric ozone pool over the eastern Mediterranean/Middle East, Atmos. Chem. Phys., 14(1), 115–132, doi:10.5194/acp-14-115-2014, 2014.

Brilli, F., Ruuskanen, T. M., Schnitzhofer, R., Müller, M., Breitenlechner, M., Bittner, V., Wohlfahrt, G., Loreto, F. and Hansel, A.: Detection of plant volatiles after leaf wounding and darkening by proton transfer reaction “time-of-flight” mass spectrometry (ptr-tof), PLoS One, 6(5), doi:10.1371/journal.pone.0020419, 2011.

Brilli, F., Gioli, B., Zona, D., Pallozzi, E., Zenone, T., Fratini, G., Calfapietra, C., Loreto, F., Janssens, I. A. and Ceulemans, R.: Simultaneous leaf- and ecosystem-level fluxes of volatile organic compounds from a poplar-based SRC plantation, Agric. For. Meteorol., 187, 22–35, doi:10.1016/j.agrformet.2013.11.006, 2014.

Cappellin, L., Karl, T., Probst, M., Ismailova, O., Winkler, P. M., Soukoulis, C., Aprea, E., Märk, T. D., Gasperi, F. and Biasioli, F.: On quantitative determination of volatile organic compound concentrations using proton transfer reaction time-of-flight mass spectrometry, Environ. Sci. Technol., 46(4), 2283–2290, doi:10.1021/es203985t, 2012.

de Gouw, J. A., Goldan, P. D., Warneke, C., Kuster, W. C., Roberts, J. M., Marchewka, M., Bertman, S. B., Pszenny, A. A. P. and Keene, W. C.: Validation of proton transfer reaction-mass spectrometry (PTR-MS) measurements of gas-phase organic compounds in the atmosphere during the New England Air Quality Study (NEAQS) in 2002, J. Geophys. Res. Atmos., 108(D21), doi:10.1029/2003JD003863, 2003.

de Gouw, J. and Warneke, C.: Measurements of volatile organic compounds in the earth’s atmosphere using proton-transfer-reaction mass spectrometry, Mass Spectrom. Rev., 26(2), 223–257, doi:10.1002/mas.20119, 2007.

Kaser, L., Karl, T., Schnitzhofer, R., Graus, M., Herdlinger-Blatt, I. S., DiGangi, J. P., Sive, B., Turnipseed, A., Hornbrook, R. S., Zheng, W., Flocke, F. M., Guenther, A., Keutsch, F. N., Apel, E. and Hansel, A.: Comparison of different real time VOC measurement techniques in a ponderosa pine forest, Atmos. Chem. Phys., 13(5), 2893–2906, doi:10.5194/acp-13-2893-2013, 2013.

Lindinger, W., Hansel, A. and Jordan, A.: On-line monitoring of volatile organic compounds at pptv levels by means of Proton-Transfer-Reaction Mass Spectrometry (PTR-MS) Medical applications, food control and environmental research, Int. J. Mass Spectrom. Ion Process., 173(3), 191–241, doi:10.1016/s0168-1176(97)00281-4, 1998.

Niinemets, Ü., Loreto, F. and Reichstein, M.: Physiological and physicochemical controls on foliar volatile organic compound emissions, Trends Plant Sci., 9(4), 180–186, doi:10.1016/j.tplants.2004.02.006, 2004.

Niinemets, Ü., Fares, S., Harley, P. and Jardine, K. J.: Bidirectional exchange of biogenic volatiles with vegetation: Emission sources, reactions, breakdown and deposition, Plant, Cell Environ., 37(8), 1790–1809, doi:10.1111/pce.12322, 2014.

Pang, X.: Biogenic volatile organic compound analyses by PTR-TOF-MS: Calibration, humidity effect and reduced electric field dependency, J. Environ. Sci. (China), doi:10.1016/j.jes.2015.01.013, 2015.

Tyrlis, E. and Lelieveld, J.: Climatology and dynamics of the summer Etesian winds over the eastern Mediterranean, J. Atmos. Sci., 70(11), 3374–3396, doi:10.1175/JAS-D-13-035.1, 2013.

Zanis, P., Hadjinicolaou, P., Pozzer, A., Tyrlis, E., Dafka, S., Mihalopoulos, N. and Lelieveld, J.: Summertime free-tropospheric ozone pool over the eastern Mediterranean/Middle East, Atmos. Chem. Phys., 14(1), 115–132, doi:10.5194/acp-14-115-2014, 2014.